Catal Lett (2009) 129:462–470
DOI 10.1007/s10562-008-9824-7

A Simple Way to Prepare C–N-Codoped TiO_2 Photocatalyst with Visible-Light Activity

Changlin Yu · Jimmy C. Yu

Received: 12 October 2008 / Accepted: 13 December 2008 / Published online: 21 January 2009

Abstract A simple method for preparing nanocrystalline C–N-codoped TiO_2 photocatalyst was developed by annealing titanium carbonitride. The prepared C–N-codoped TiO_2 powders were characterized by TGA, XRD, XPS, UV–Vis, PL, SEM, and BET surface areas. The photocatalytic activity was evaluated by the photocatalytic degradation of methylene blue in an aqueous solution under visible-light radiation. Results showed that the annealing temperatures and time affected the crystal composition and structure and activity of the catalyst. The most promoting effect of C–N-codoping in activity was obtained over C–N-codoped TiO_2 prepared by annealing titanium carbonitride at 400 °C for 8 h. The high photocatalytic activity could be attributed to the synergetic effects in light absorption and the suppression of recombination of electrons/holes pairs.

Keywords Titanium carbonitride · C–N-codoped TiO_2 · Degradation of methylene blue · Photocatalysis

1 Introduction

TiO_2 is the most attractive photocatalyst due to its high oxidative power, photostability, low cost, and nontoxicity [1]. However, the anatase TiO_2 needs UV for activation due to its large band gap of 3.2 eV. Pure TiO_2 is therefore not effective for solar-driven applications. Many approaches have been proposed to overcome this limitation. For example, carbon-doped TiO_2 was found to be effective for water splitting under visible light [2, 3]. Asahi et al. [4] calculated the band structure of nitrogen-doped TiO_2 and studied the visible-light photocatalytic degradation of acetaldehyde and methylene blue (MB). Hashimoto et al. reported the visible-light-induced hydrophilicity [5] and photocatalytic decomposition of gaseous 2-propanol on nitrogen-doped TiO_2 [6]. They concluded that the lattice oxygen sites were substituted by nitrogen atoms and formed an isolated narrow band above the valence band.

Doping of other nonmetals such as S, F, and B has also been investigated [7–10]. Sulfur could be doped as an anion and replaced the lattice oxygen in TiO_2 [11–13]. F-doping could result in the creation of surface oxygen vacancies [14], and boron atoms can substitute oxygen atoms in the TiO_2 lattice and the *p* orbital of B is mixed with O 2*p* orbital, which causes the band-gap narrowing [15].

More recently, nonmetal codoping presents a promising strategy to further enhance the visible-light activity of TiO_2 [16, 17]. Xie et al. [17] have reported that F–N-codoped samples exhibit much higher visible-light-induced catalytic activities than that of Degussa P25 and the as-prepared pure TiO_2. This property can be attributed to the synergetic effects of absorption in the visible-light region causing red shift in the adsorption edge. N-doping into TiO_2 resulted in the creation of surface oxygen vacancies, and F-doping produced several beneficial effects, including the creation of surface oxygen vacancies, the enhancement of surface acidity and the Ti^{3+} ions [14]. Chen et al. [18] have reported the C–N-TiO_2 nanomaterials with different

C. Yu (✉)
School of Materials and Chemical Engineering,
Jiangxi University of Science and Technology,
341000 Ganzhou, People's Republic of China
e-mail: yuchanglinjx@163.com

J. C. Yu
Department of Chemistry, The Center of Novel Functional Molecules, and Environmental Science Programme,
The Chinese University of Hong Kong, Shatin,
New Territories, Hong Kong, China

nitrogen and carbon contents prepared by a sol–gel method, which exhibited the highest photocatalytic activity, which could be assigned to the synergistic effect of doped C and N atoms. This synergetic effect can promote the absorption enhancement in the visible region and adsorption of organic reactant, and thus the photocatalytic reaction under visible irradiation can be accelerated.

In this study, we developed a simple and effective method for the synthesis of C–N-codoped TiO_2 photocatalysts by the oxidative annealing of the titanium carbonitride compounds in air. The most attractive feature of our method is that titanium carbonitride is used as both a precursor of titanium dioxide and a carbon and nitrogen source for the simultaneous crystallization and doping.

2 Experimental

2.1 Sample Preparation

Carbonitride powders (1–2 μm, 99% Ti_2CN) used in this study was supplied from Aldrich and was used as received. About 1 g carbonitride was placed in a furnace (Vulcan 3–1750) and then calcined at different temperatures and time in air with a heating rate of 3 °C/min. After the calcination, the black carbonitride compound converted to C–N-codoped TiO_2 photocatalysts. The color of the C–N-codoped TiO_2 photocatalysts vary from deep yellow to shallow yellow, which depends on the calcination temperature. P25 TiO_2 (ca. 80% anatase, 20% rutile) was obtained from the Degussa Co. (Dossenheim, Germany).

2.2 Catalyst Characterization

The Brunauer–Emmett–Teller (BET) surface areas of the sample was obtained from N_2 adsorption/desorption isotherms determined at liquid nitrogen temperature on an automatic analyzer (ASAP 2010). The samples were outgassed for 2 h under vacuum at 180 °C prior to adsorption.

X-ray diffraction (XRD) patterns, obtained on a Bruker D8 Advance X-ray diffractometer using CuKα radiation at a scan rate of 0.05° (2θ) s^{-1}, were used to identify the phase constitution in samples and their crystallite size. The accelerating voltage and the applied current were 40 kV and 40 mA, respectively. The crystallite size was calculated from X-ray line broadening analysis by the Scherrer formula.

Differential thermogravimetric analysis (TGA) was recorded on a Thermal Analy TGA 2950 instrument at air atmosphere with the heating rate of 10 °C/min.

UV–Vis diffuse reflectance spectra were achieved using a UV–Vis spectrophotometer (Cary 100 scan spectrophotometers, Varian). Absorption spectra were referenced to $BaSO_4$.

The microstructures of the samples were determined by using an S-360 (Cambridge) Scanning Electron Microscope.

To investigate the recombination and lifespan of photogenerated electrons/holes in the photocatalysts, the photoluminescence (PL) emission spectra of the samples were recorded. A 325 nm He–Cd laser was used as an excitation light source. The emission from the sample was measured by a spectrometer (Spex 500 M, USA) equipped with a photon counter (SR400, USA).

The samples were also analyzed by X-ray photoelectron spectroscopy on a PHI Quantum 2000 XPS System with a monochromatic AlKa source and a charge neutralizer. All the binding energies were referenced to the C 1*s* peak at 284.8 eV of the surface adventitious carbon.

2.3 Photocatalytic Activity Measurement

The photocatalytic activities of the C–N-codoped TiO_2 samples were determined by measuring the degradation of MB in an aqueous solution under visible-light irradiation. The experimental setup of the activity test is according to literatures [19, 20], as shown in Fig. 1. A 300 W tungsten lamp was positioned inside a cylindrical Pyrex vessel surrounded by a circulating cooling water jacket and a cutoff filter solution jacket (HCl aqueous solution of $CuSO_4$ (0.5 M) and K_2CrO_4 (0.002 M) which cuts off wavelengths shorter than 400 nm and longer than 660 nm. The photocatalyst (0.05 g) was suspended in 80 mL aqueous solution of $C_0 = 0.008$ g/L. Before the lamp was turn on, the suspension was stirred in the dark for 40 min. The suspension was vigorously stirred with the photoreactor during the process and the temperature of suspension

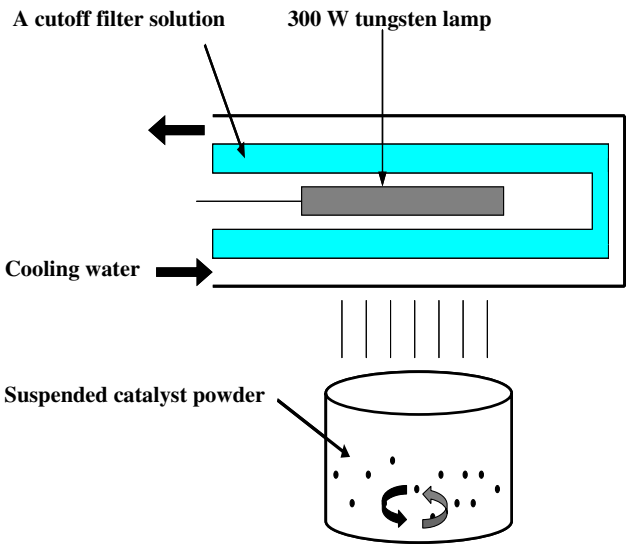

Fig. 1 Schematic diagram of the experimental setup of the activity test under visible-light irradiation

was maintained at 22 ± 2 °C by circulation of water through an external cooling coil. After reacting, the sample of suspension was taken out and centrifuged. The clear upper layer solution was analyzed by a Milton Roy Spectronic 3000 Array spectrophotometer (New York, USA). The dye concentration was measured at $\lambda = 663$ nm, the maximum absorption wavelength for MB.

3 Results and Discussion

3.1 Crystal Characterization

XRD was used to investigate the phase constitution of the Ti_2CN powders annealed in air at different temperatures and time. The results are shown in Fig. 2. The phase content of a sample was calculated from the integrated intensities of anatase (101) and rutile (110) peaks according to literatures [21, 22]. If a sample contains anatase and rutile, the mass fraction of anatase (W_A) and rutile (W_R) can be calculated from the Eqs. (1) and (2) [22]

$$W_A = \frac{K_A A_A}{K_A A_A + A_R} \quad (1)$$

$$W_R = \frac{A_R}{K_A A_A + A_R} \quad (2)$$

where A_A and A_R are the integrated intensity of the anatase (101) and rutile (110) peaks, respectively, W_A and W_R represent the mass fraction of anatase and rutile, respectively, and K_A is coefficients and its value is 0.886. The average crystallite sizes of anatase were determined according to the Scherrer equation using the fwhm data of each phase after correcting the instrumental broadening [21, 22]. The calculation results of crystallite size and crystal phase are summarized in Table 1.

From Table 1, we can see that the crystalline size of anatase in P25 is about 28 nm. When the Ti_2CN powders were annealed at 400 °C in air for 4–12 h, the products were pure anatase with about a crystallite size of about 22 nm. The rutile phase appeared when the calcination temperature was increased to 500 °C. Under this treatment temperature, the rutile content was about 24% and the crystallite size increased to 27 nm. If the temperature was further increased to 700 °C, the peak intensities of anatase increased and the width of the (101) plane diffraction peak of anatase ($2\theta = 25.4^0$) became narrower. The crystallite size in the sample calcined at 700 °C was around 35 nm.

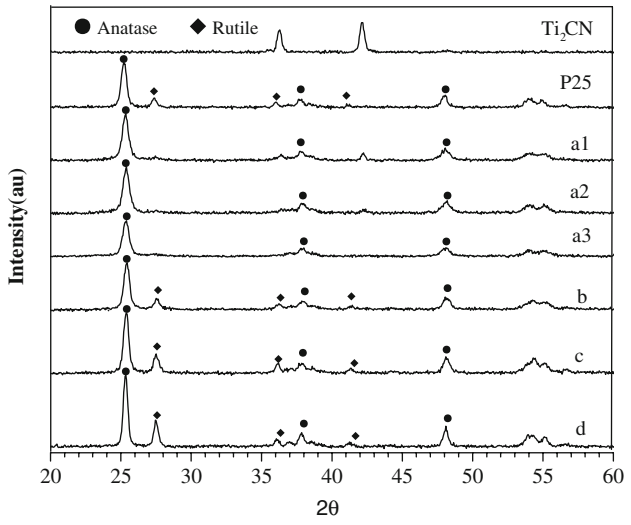

Fig. 2 XRD pattern of the sample Ti_2CN powders annealed in air for *a1* 4 h at 400 °C, *a2* 8 h at 400 °C, *a3* 12 h at 400 °C, *b* 4 h at 500 °C, *c* 4 h at 600 °C, *d* 4 h at 700 °C

3.2 Specific Surface Area Analysis

Table 1 shows BET specific surface area and pore volume of TiO_2 powders prepared at different calcination temperatures and time. All samples show the lower specific surface area and pore volume than those of P25. Calcination temperatures show great effects on the pore structure and surface area of sample. The S_{BET} values and pore volume decrease greatly with increasing calcination temperatures due to crystallite growth and sintering. At 700 °C, the values of S_{BET} and pore volume of the sample decrease to 5.76 m^2/g and 0.022 cm^3/g, respectively. The S_{BET} value is only one quarter of the sample prepared at

Table 1 Surface areas, pore volume of pores, crystalline size, crystal phase in the samples

Sample	Surface area[a] (m^2/g)	Pore volume[b] (cm^3/g)	Crystalline size[c] (nm)	Crystal phase[d]
P25	54.72	0.220	28	80% A, 20% R
a1	23.66	0.046	24	100% A
a2	21.90	0.045	21	100% A
a3	21.31	0.044	22	100% A
b	13.86	0.038	27	85% A, 15% R
c	9.34	0.035	29	75% A, 25% R
d	5.76	0.022	35	73% A, 27% R

Ti_2CN powders annealed in air for (a1) 4 h at 400 °C, (a2) 8 h at 400 °C, (a3) 12 h at 400 °C, (b) 4 h at 500 °C, (c) 4 h at 600 °C, (d) 4 h at 700 °C

[a] BET surface area calculated from the linear part of the BET plot ($P/P_0 = 0.05$–0.3)

[b] Total pore volume, taken from the volume of N_2 adsorbed at $P/P_0 = 0.995$

[c] Calculated from X-ray line broadening analysis by Scherrer formula from XRD result from anatase phase

[d] A and R denote anatase and rutile, respectively

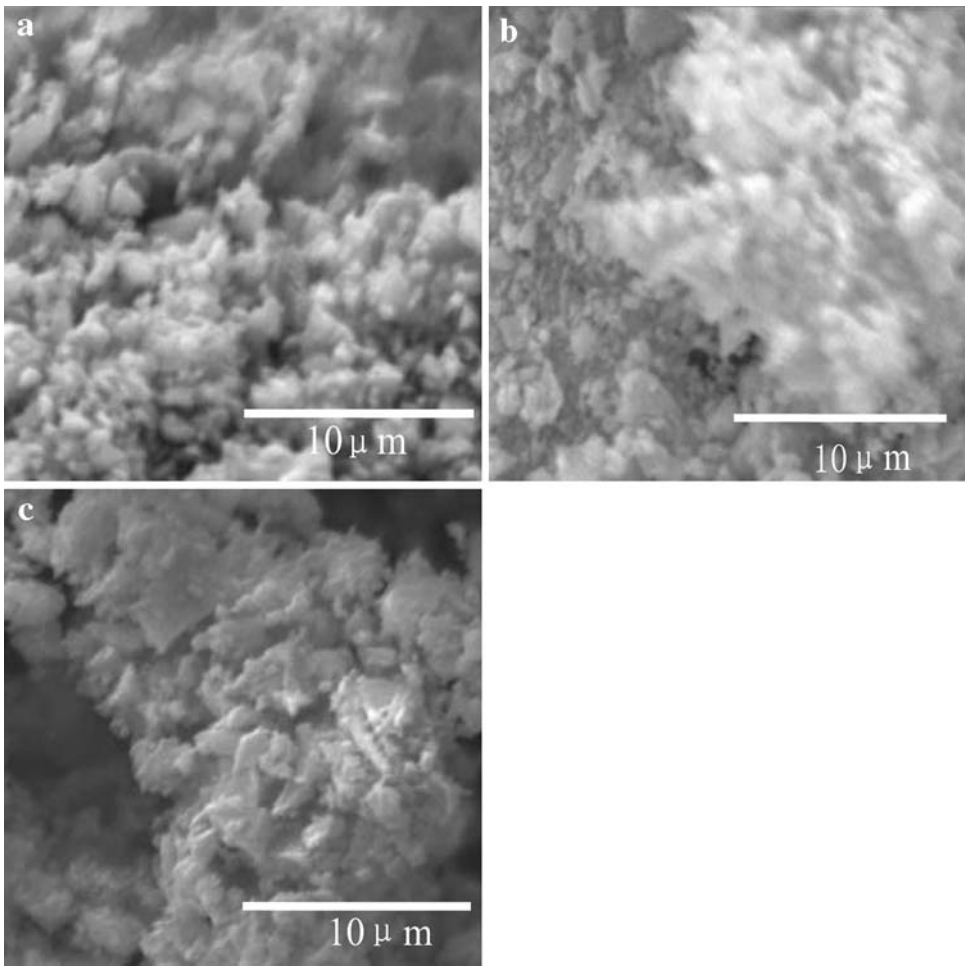

Fig. 3 SEM images of the different catalysts. **a** Ti_2CN powders annealed in air for 4 h at 400 °C, **b** 8 h at 400 °C, **c** 4 h at 700 °C

400 °C. However, when the temperature was maintained at 400 °C, the BET specific surface area and pore volume show no obvious changes with increasing calcination time.

3.3 SEM Analysis

Figure 3 shows SEM photographs of TiO_2 powders prepared at 400 and 700 °C. As shown in Fig. 2 (a1, a2, a3, b), the TiO_2 particles are uniform and well dispersed, which indicates that the aggregation of the particles is negligible at 400 °C. Usually, the pores within the hard aggregates give the intra-particle pores, while the voids between these aggregates give the inter-particle pores. With increasing calcination temperature, the particle size of aggregates increases, which results in inter-particle pores becoming stronger and then causing the decrease of pore volume. From Fig. 3c, we can see that much bigger particles appear and these particles are not well dispersed. At 700 °C, the particles are easily aggregated due to the sintering reaction among small particles.

3.4 TGA Analysis

In order to investigate the reaction of Ti_2CN powders in air, TGA measurements were carried out. The results are shown in Fig. 4. As expected, the Ti_2CN powders can be oxidized by oxygen in the air at an elevated temperature of >350 °C. From 350 to 600 °C, the total weight increase is about 30%. If all carbon and nitrogen were oxidized, the weight increase would be 31.25% as calculated from the reaction: $Ti_2CN + 4O_2 \rightarrow 2TiO_2 + CO_2 + NO_2$. The amounts of residual carbon and nitrogen are dependent on the annealing temperature.

3.5 XPS Analysis

XPS measurements were carried out to determine the chemical composition of the samples and the valence states of various species present therein. Figure 5 represents the high-resolution XPS spectra of the C 1*s*, N 1*s*, O 1*s*, and Ti 2*p* regions of pure Ti_2CN and C–N-codoped TiO_2. In the case of the pure Ti_2CN powder, the C 1*s* spectrum is

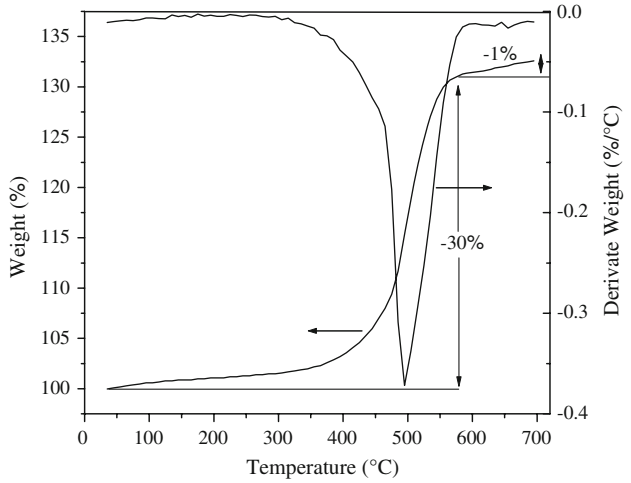

Fig. 4 TGA profile of Ti_2CN powders in air

composed of three peaks at 281, 284, and 287 eV. Based on previous studies [23–25], the former two signals were assigned to the C 1*s* peaks from Ti–C (282 eV) and C–C (285 eV) bonds. The shoulder peak around 287 eV in the three spectra is ascribed to the C atoms of a carbonate compound [26]. In the spectrum of the C–N-codoped TiO_2, some shifts were observed in these peaks. For the sample calcined at 400 °C for 8 h, it may reasonable to ascribe the first peak (284 eV), second peak (286 eV), and last peak (288 eV) to Ti–C and C–C (285.3 eV) and bonds the C atoms of a carbonate compound, respectively. However, second peak (C–C) was not observed. The intensity of the C 1*s* peak in the sample calcined at 700 °C is much weaker than that in the other two samples. Figure 5b shows the N1*s* core level photoelectron spectrum of the three samples. In the pure Ti_2CN sample, the peak around 396 eV

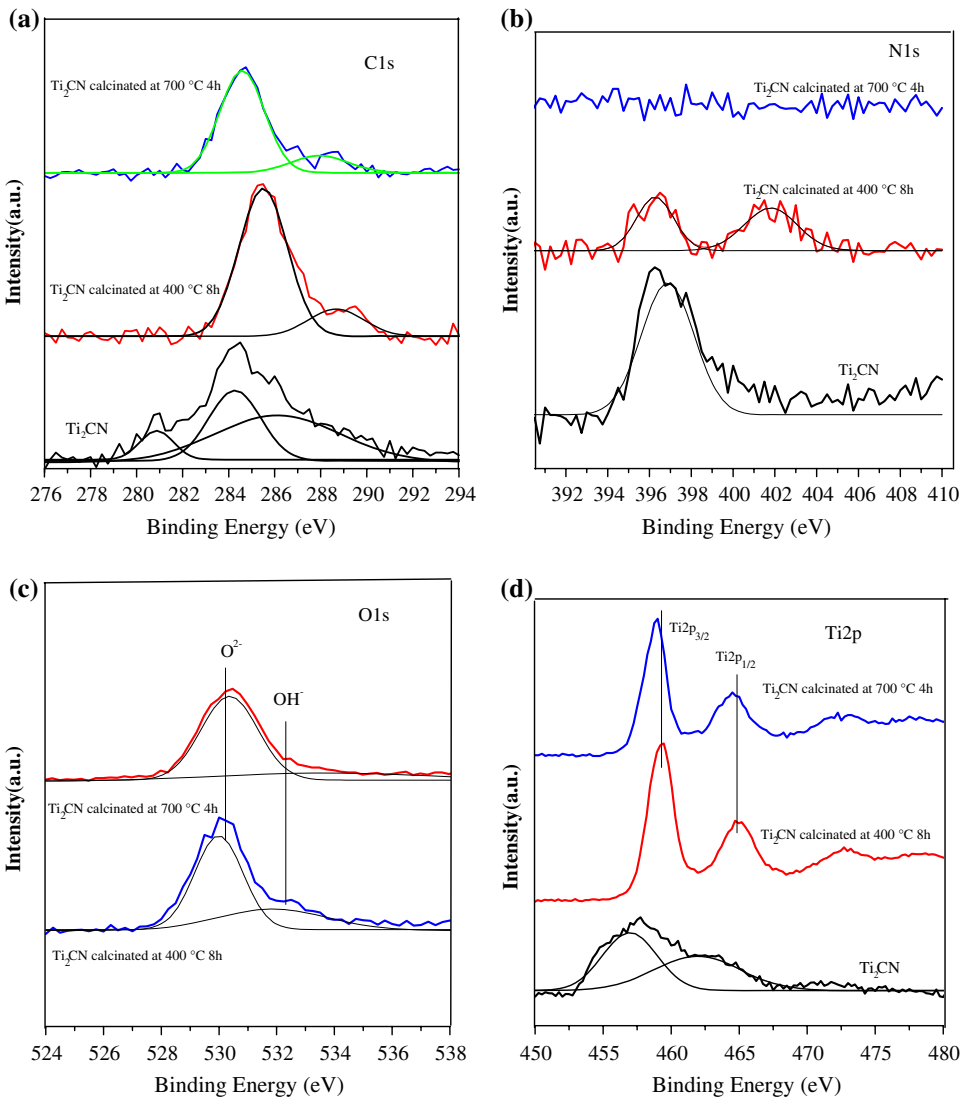

Fig. 5 XPS spectra for the **a** C 1*s*, **b** N 1*s*, **c** O 1*s* and **d** Ti 2*p* of samples

can be attributed to Ti–N bonds [27, 28]. However, in the spectrum of C–N-codoped TiO_2 prepared at 400 °C, two weak peaks can be discerned. The new N 1*s* peak at 400–403 eV may be related to the formation of the N–Ti–O linkages [29] or NO-like species [30]. When the Ti_2CN was calcined at 700 °C, no nitrogen species could be detected.

Figure 5c shows the O 1*s* core level photoelectron spectrum of the two calcined samples. By curve fitting, the peak at 530 eV corresponds to lattice oxygen of TiO_2, and a shoulder located at higher binding energy of 532 eV is assigned to mixed contributions from surface hydroxides [31, 32]. There are more surface hydroxides over the sample calcined at 400 °C than those over the sample calcined at 700 °C. The spin–orbit components ($2p_{3/2}$ and $2p_{1/2}$) of Ti 2*p* peaks over the calcined two samples are well deconvoluted by two curves at 459 and 464 eV (Fig. 5d) with a split of 5 eV between the doublets, indicating that Ti exists in the Ti^{4+} form [33]. The signals at 457.0 and 462.0 eV observed in pure Ti_2CN could be ascribed to the titanium oxides due to air oxidization of Ti_2CN [23].

3.6 Diffuse Reflectance UV–Vis Spectroscopy

Figure 6 shows the UV–Vis diffuse reflectance spectra of P25 and N–C-codoped TiO_2. P25 practically does not absorb visible-light, whereas the codoping of nitrogen and carbon greatly extends the absorption edges to the visible-light region. Sample a1 calcined at 400 for 4 h exhibits the largest visible-light absorption in the seven samples, and its absorption edge shifts to longest wavelength (λ = 510 nm). The absorption edge shifts toward longer wavelengths for all C–N-doped TiO_2 powders. This clearly indicates a decrease in the band-gap energy of TiO_2. The edge energies for the present series of catalysts were determined with Tauc's law from the intercept of a straight line fitted through the rise of the function $[F(Ra)hm]^2$ plotted versus *hm*, where *F(Ra)* is a Kubelka–Munk function [34, 35] and *hm* is the energy of the incident photon. The values obtained for the dehydrated catalysts are listed in Table 2. The estimated band-gap energies for samples prepared with Ti_2CN are lower than that for P25 (E_g = 3.02 eV) suggesting that the C–N-codoped TiO_2 photocatalysts are more active than P25 under visible-light.

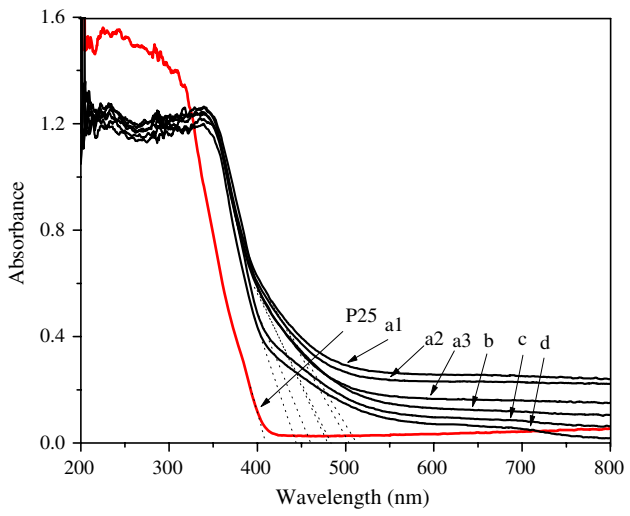

Fig. 6 UV–Vis absorption spectra of the samples. Ti_2CN powders annealed in air for *a1* 4 h at 400 °C, *a2* 8 h at 400 °C, *a3* 12 h at 400 °C, *b* 4 h at 500 °C, *c* 4 h at 600 °C, *d* 4 h at 700 °C

3.7 Photoluminescence Spectra and Electron/Hole Recombination

Photoluminescence (PL) emission spectra can be used to investigate the efficiency of charge carrier trapping, immigration and transfer, and to understand the fate of electron/hole pairs in semiconductor particles [36]. In order to study the effects of C–N codoping on the recombination of photogenerated electron/hole pairs, the PL spectra were recorded. The peak position of the emission band for rutile powder is about 450 nm and that of anatase powder is about 500 nm [37]. In this study, the PL emission spectra of all samples were examined in the wavelength range of 330–600 nm. From Fig. 7, we can see that the peak position of the emission band appears around 400 nm. The intensity of the PL spectra for C–N codoped TiO_2 samples is lower than that of pure TiO_2. Since the observed PL spectrum in TiO_2 can be attributed to the radiative recombination process of self-trapped excitations [37–40], or hydroxylated Ti^{3+} surface complexes [41] from the charge transfer excited state of the highly dispersed titanium oxide species, the reduction of PL intensity in the sample C–N codoped TiO_2 indicates the decrease of the radiative recombination process. However, the emission intensity is closely related to the calcination time and

Table 2 The absorption edge (λ_g) and estimated band-gap energy (E_g)

Sample	λ_g (nm)	E_g (eV)
P25	410	3.02
a1	510	2.43
a2	502	2.47
a3	481	2.58
b	479	2.59
c	459	2.70
d	443	2.80

Ti_2CN powders annealed in air for (a1) 4 h at 400 °C, (a2) 8 h at 400 °C, (a3) 12 h at 400 °C, (b) 4 h at 500 °C, (c) 4 h at 600 °C, (c) 4 h at 700 °C

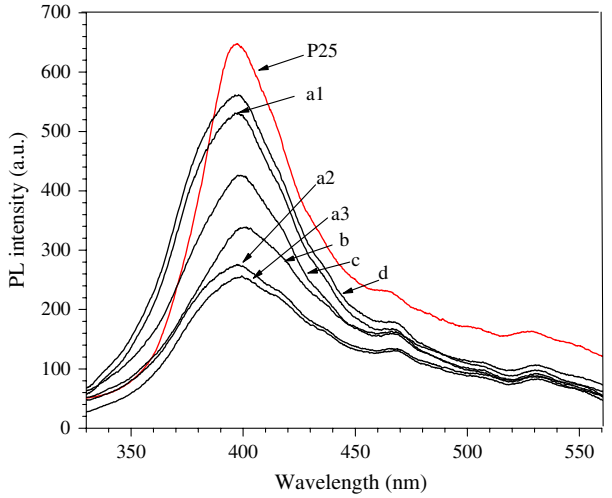

Fig. 7 The photoluminescence (PL) spectra of the samples. Ti_2CN powders annealed in air for *a1* 4 h at 400 °C, *a2* 8 h at 400 °C, *a3* 12 h at 400 °C, *b* 4 h at 500 °C, *c* 4 h at 600 °C, *d* 4 h at 700 °C

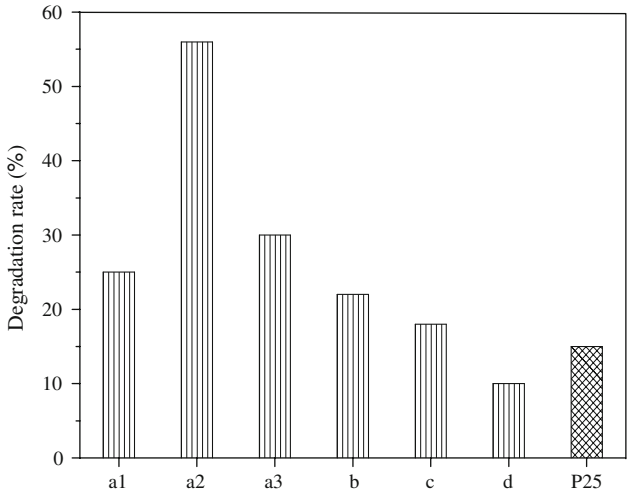

Fig. 8 Photocatalytic activity comparison of the different catalysts under visible-light radiation. Reaction time: 3 h Ti_2CN powders annealed in air for *a1* 4 h at 400 °C, *a2* 8 h at 400 °C, *a3* 12 h at 400 °C, *b* 4 h at 500 °C, *c* 4 h at 600 °C, *d* 4 h at 700 °C

calcination temperatures. The emission intensity of sample a1 is much stronger than sample a2 and a3. This is because the short calcination time leads to a higher concentration of C and N in sample a1. The high concentration of C and N could produce new defect sites which enhance the recombination of photogenerated electrons and holes [6]. Prolonging the calcination time at this temperature could keep an appropriate amount of C and N doping. This may slow down the radiative recombination process. A similar phenomenon was observed for F-doping [10]. It takes about 100 ns for electron to migrate from the interior of a 1 μm TiO_2 to its surface [42]. When the particle size is shrinked to 10 nm, this process needs only about 10 ps. A nanosized photocatalyst is often more photoactive because a fast electron removal can minimize electron–hole pair recombination.

3.8 Photocatalytic Activity in the Degradation of Methylene Blue

The photocatalytic activities of C–N-codoped TiO_2 were evaluated by using the degradation of MB under visible-light radiation. For comparison, the activity of pure TiO_2 (P25) was tested under the same conditions. Figure 8 shows the comparison of the degradation rate for the different photocatalysts under visible-light radiation for 3 h. Only very weak photodegradation activity of P25 was observed. The main reason for the activity could be the sensitization mechanism of MB since the absorption of P25 at $\lambda > 400$ nm is very weak. This mechanism involves charge injection from excited dye into photocatalysts and subsequent degradation of oxidized dye. From this figure, we can find that C–N codoped amples prepared by annealing at 400 °C (samples a1, a2, and a3) show a comparatively high decomposition rate. Among them, sample a2 prepared by annealing the Ti_2CN powders at 400 °C for 8 h gives the highest photocatalytic activity. The value of degradation rate for sample a2 is about 55% after 3 h irradiation. The elevated temperature treatment at 600 or 700 °C leads to a decrease in photocatalytic activity, which could be attributed to the loss of doped nitrogen element and the deteriorated texture of catalyst, such as the loss of surface area, an increase in crystalline size and an increased rate of electron–hole recombination.

3.9 Mechanism for the Enhancement of the Photocatalytic Activity of TiO_2 by C–N Codoping

Nonmetal doped TiO_2 has received great attention because of its potential application in solar-driven photocatalysis. Asahi et al. [4] found that nitrogen atoms substituted the lattice oxygen sites of TiO_2 and narrowed the band gap by mixing the N 2*p* and O 2*p* states. Other theories have been proposed recently to explain the nonmetal doping effect. Irie et al. [3] observed that quantum yields for the decomposition of gaseous 2-propanol on N-doped TiO_2 were significantly enhanced from irradiating with ultraviolet light, compared with those from irradiating with visible light. They suggested that the visible-light response in N-doped TiO_2 might be due to the N 2*p* states isolated above the valence-band maximum of TiO_2, rather than due to a band-gap narrowing. Lee et al. [43] applied the first-principles density-functional calculations to account for the electronic properties of N-doped and C-doped TiO_2. They found bands originating from N(C) 2*p* states in the band

gap of TiO_2. The absorption of visible light was due to the isolated N 2*p* states above the valence-band maximum of TiO_2 rather than from band-gap narrowing. By utilizing the deep-level optical spectroscopy measurements, Nakano et al.[44] revealed three deep levels located at ~0.86, ~1.30, and ~2.34 eV below the conduction band over C-doped TiO_2 films. The first level was probably attributable to the intrinsic nature of TiO_2, whereas the latter two levels were newly introduced by the C-doping. In particular, the pronounced 2.34 eV band contributed to band-gap narrowing by mixing with the O 2*p* valence band.

Excluding the influences of the self sensitization of MB, we tentatively suggested a simple mechanism, as shown in Fig. 9. In the C–N-codoped TiO_2 catalyst, there may exist the isolated N(C) 2*p* states above the valence-band maximum of TiO_2, which result in the strong absorption enhancement in the visible region. Irradiating with visible light excites electrons in the narrow bands. The electrons move to the surface and further transfer to oxygen adsorbed on the surface producing O_2^-, which can further transform to H_2O_2 and $OH^\bullet$, resulting in the oxidation of MB at last [45]. On the other hand, the reactive holes (h^+) oxidize MB either directly or through a primarily formed $OH^\bullet$ produced by the oxidation of ubiquitous water. An appropriate N and C atom doping could reduce the recombination of electrons/holes pair, then further increasing photocatalytic activity. Our adsorption experiment of MB on different samples indicated that the amount of MB adsorbed on the C–N-codoped TiO_2 catalyst is obviously higher than that of P25 (shown in Fig. 10), similar to Chen's report [18]. The increase amount of MB over the surface will more effectively utilize the photoexcitons. Furthermore, the

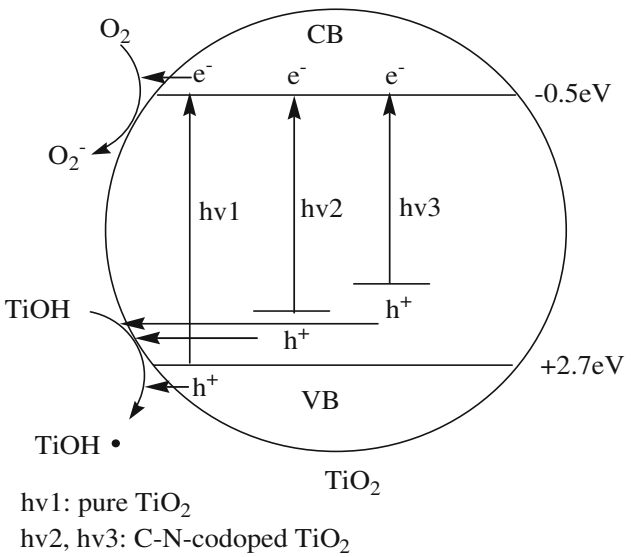

Fig. 9 Possible mechanism of C–N-codoped TiO_2 light photocatalysis

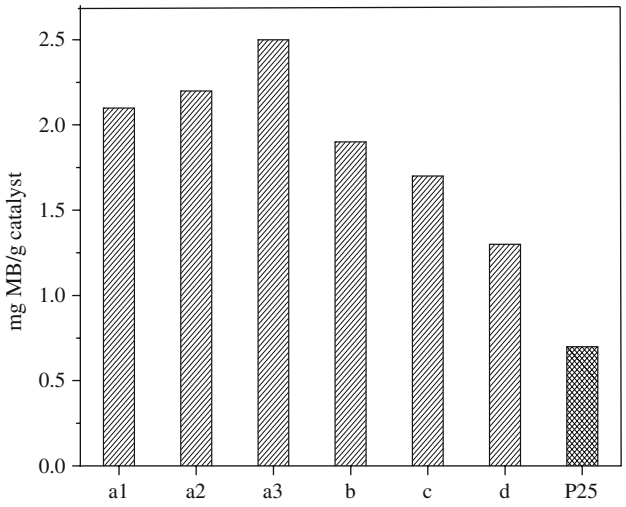

Fig. 10 The results of the adsorption of MB on the samples

carbonaceous species formed at the surface of TiO_2 samples could be capability of exciting by visible-light-like organic dyes, as suggested by Sakthivel [3]. Although the main cause of the noted C–N-codoping effects is not very clear at this stage, it provide an effective way to prepare the efficient C–N-codoped TiO_2 catalyst.

4 Conclusions

A simple method was developed for simultaneous doping of carbon and nitrogen in TiO_2 by annealing titanium carbonitride in air. These catalysts show high photoactivity under visible-light irradiation. The C–N-codoping can reduce the band-gap energy and promote the adsorption of visible light. It can also reduce the electron/hole pair recombination rate. The calcination temperatures and treatment time play an important role in the structure and activity of the catalysts. C–N-codoped TiO_2 powders prepared by annealing Ti_2CN at 400 °C for 8 h exhibit the highest photocatalytic activity.

Acknowledgments This work was co-supported by the initial fund for new researcher of Jiangxi University of Science and Technology and a strategic investments scheme administrated by The Chinese University of Hong Kong

References

1. Sulikowski B, Haber J, Kubacka A, Pamin K, Olejniczak Z, Ptaszynski J (1996) Catal Lett 39:27
2. Khan SUM, Al-Shahry M, Ingler WB Jr (2002) Science 297:2243
3. Sakthivel S, Kisch H (2003) Angew Chem Int Ed 42:4908
4. Asahi R, Morikawa T, Ohwaki T, Aoki K, Taga Y (2001) Science 293:269
5. Irie H, Washizuka S, Yoshino N, Hashimoto K (2003) Chem Commun 1298

6. Irie H, Watanabe Y, Hashimoto K (2003) J Phys Chem B 107:5483
7. Yu JC, Ho WK, Yu JG, Yip HY, Wang PK, Zhao JC (2005) Environ Sci Technol 39:1175
8. Ho WK, Yu JC, Lee SC (2006) J Solid State Chem 179:1171
9. Ho WK, Yu JC, Lee S C (2006) Chem Commun 1115
10. Yu JC, Yu JG, Ho WK, Jiang ZT, Zhang LZ (2002) Chem Mater 14:3808
11. Umebayashi T, Yamaki T, Itoh H, Asai K (2002) Appl Phys Lett 81:454
12. Umebayashi T, Yamaki T, Tanala S, Asai K (2003) Chem Lett 32:330
13. Umebayashi T, Yamaki T, Yamamoto S, Miyashita A, Tanala S, Sumita T, Asai K (2003) J Appl Phys 93:5156
14. Li D, Haneda H, Hishita S, Ohashi N (2005) J Solid State Chem 178:3293
15. Zhao W, Ma WH, Chen CC, Zhao JC, Shuai ZG (2004) J Am Chem Soc 16:4782
16. Yu JG, Zhou MH, Cheng B, Zhao XJ (2006) J Mol Catal A Chem 246:176
17. Xie Y, Li YZ, Zhao XJ (2007) J Mol Catal A Chem 277:119
18. Chen DM, Jiang ZY, Geng JQ, Wang Q, Yang D (2007) Ind Eng Chem Res 46:2741
19. Ho WK, Yu JC, Lin J, Yu JG, Li PS (2004) Langmuir 20:5865
20. Yu JC, Li GS, Wang XC, Hu XL, Leung CW, Zhang ZD (2006) Chem Commun 2717
21. Yu JC, Yu JG, Zhang LZ, Ho WK (2002) J Photochem Photobiol A Chem 148:263
22. Zhang H, Banfield JF (2000) J Phys Chem B 104:3481
23. Santerre F, Khakani MAE, Chaker M, Dodelet JP (1999) Appl Surf Sci 148:24
24. Baba K, Hatada R (2001) Surf Coat Technol 136:241
25. Choi Y, Umebayashi T, Yamamoto S, Tanaka S (2003) J Mater Sci Lett 22:1209
26. Christi AB, Sutherland I, Walls JM (1981) Vacuum 31:513
27. Kobayakawa K, Murakami Y, Sato Y (2005) J Photochem Photobiol A 170:177
28. Mi YY, Wang SJ, Chai JW, Pan JS, Huan CHA, Feng YP, Ong CK (2006) Appl Phys Lett 89:231922
29. Wang X, Yu JC, Chen Y, Wu L, Fu X (2006) Environ Sci Technol 40:2369
30. Chen H, Nambu A, Wen W, Graciani J, Zhong Z, Hanson JC, Fujita E, Rodriguez JA (2007) J Phys Chem C 111:1366
31. Mcafferty E, Wightman JP (1998) Surf Interface Anal 26:549
32. Erdem B, Hunsicker RA, Simmons GW, David Sudol E, Dimonie VL, El-Aasser MS (2001) Langmuir 172:664
33. Reddy BM, Rao KN, Reddy GK, Bharali P (2006) J Mol Catal A Chem 25:344
34. Kormann C, Bahnemann DW, Hoffmann MR (1988) J Phys Chem 92:5196
35. Yu JG, Yu JC, Ho WK, Jiang ZT (2002) New J Chem 26:607
36. Yu JG, Yu HG, Cheng B, Zhao XJ, Yu JC, Ho WK (2003) J Phys Chem B 107:13871
37. Li XZ, Li FB, Yang CL, Ge WK (2001) J Photochem Photobiol A Chem 141:209
38. Fujihara K, Izumi S, Ohno T, Matsumura M (2000) J Photochem Photobiol A Chem 132:99
39. Yang C, Wohlgenannt M, Vardeny ZV, Blau WJ, Dalton AB, Baughman R, Zakhidov AA (2003) Physica B 338:366
40. Yu Y, Yu JC, Yu JG, Kwok YC, Che YK, Zhao JC, Ding L, Ge WK, Wong PK (2005) Appl Catal A 289:186
41. Anpo M, Alkawan N, Kubokaway Y (1985) J Phys Chem 89(23):5017
42. Lewis NS (1991) Annu Rev Phys Chem 42:543
43. Lee JY, Park JW, Cho JH (2005) Appl Phys Lett 87:011904
44. Nakano Y, Morikawa T, Ohwaki T, Taga Y (2005) Appl Phys Lett 87:052111
45. Dibble LA, Raupp GB (1990) Catal Lett 4:345